Shellac-based encapsulation model incorporating calcium fluoride for oral care applications

Piyada Dissara[1], Chompunuch Sukcheep[2], Sanong Ekgasit[3], Prompong Pienpinijtham[3]*, and Apichat Phengdaam[4]*

ABSTRACT

Fluoride-releasing systems are widely incorporated into dental products to prevent caries; however, fluoride ions readily interact with calcium compounds in oral formulations, resulting in deactivation and reduced effectiveness. To overcome this limitation, a simple extrusion method was designed to fabricate shellac-based biopolymer beads capable of encapsulating fluoride. The resulting beads had an average diameter of 2.54 ± 0.22 mm, with theoretical analysis supporting particle size dependence on extrusion tube diameter. Structural and stability characterization was conducted using optical and electron microscopy, elemental analysis, vibrational spectroscopy, and thermal profiling, confirming *in situ* calcium fluoride formation and effective pore sealing. Key formulation parameters—including shellac concentration, dissolution time, bead formation time, and hardening time—were optimized to improve bead morphology and fluoride retention. An *in situ* blocking strategy, involving controlled precipitation of calcium fluoride within the bead matrix during formulation, was implemented to minimize fluoride diffusion and enhance long-term stability. This approach achieved 70% active fluoride retention over 90 days. The proposed encapsulation model holds promise for applications in toothpaste and other dental care products.

Keywords:
Biopolymer; Calcium fluoride; CaF_2; Encapsulation; Fluoride; Shellac

***Corresponding authors:**
Prompong Pienpinijtham, prompong.p@chula.ac.th;
Apichat Phengdaam, apichat.p@psu.ac.th

How to cite this article:
Dissara, P., Sukcheep, C., Ekgasit, S., Pienpinijtham, P., Phengdaam, A. Shellac-based encapsulation model incorporating calcium fluoride for oral care applications. *Biomater Transl.* 2025.

doi: 10.12336/bmt.25.00099

1. Introduction

Fluoride plays a fundamental role in the prevention of dental caries by facilitating mineralization of calcium ions released from damaged hydroxyapatite in enamel, leading to the precipitation of fluorapatite, hydroxyfluorapatite, and calcium fluoride (CaF_2).[1,2] Dental fluoride products are widely utilized to enhance oral health and inhibit dental caries.[3] These products range from commercial dental materials with integrated fluoride, such as composites, adhesives, and cements,[4] to slow-release devices for sustained fluoride exposure.[5] Professional applications include high-concentration fluoride solutions, gels, pastes, and varnishes. For home use, fluoridated toothpastes and mouthwashes provide accessible fluoride exposure and form an essential part of daily oral hygiene routines.[6] Chewing gums that contain fluoride combine increased fluoride exposure with stimulated salivary flow to provide greater cariostatic effects.[3,7] Advances in microencapsulation technology have further improved medicated chewing gums by enabling the controlled release of active ingredients within the gum matrix.[8]

Unfortunately, fluoride ions (F^-) can interact with calcium ions (Ca^{2+}) present in compounds such as calcium phosphate and calcium carbonate, which are commonly found in toothpaste and other dental products. F^- reacts strongly with calcium abrasives, causing a 60–90% loss of active fluoride. Although silicate or kaolin abrasives preserve some fluoride, a significant portion still converts into inactive forms, reducing effectiveness.[9] This interaction leads to fluoride deactivation and reduced efficacy.[10] Although various encapsulation methods have been explored, they frequently exhibit inconsistent

encapsulation efficiency and fluoride release profiles, which compromise their clinical utility. Encapsulation, defined as the entrapment of active agents within a carrier matrix,[11] offers a promising strategy for preserving fluoride in its active form. In the present study, a bead-based encapsulation system was selected using a biopolymer due to its biocompatibility, high surface-to-volume ratio, favorable flow properties, and feasibility in manufacturing and handling processes.[12,13] Notably, mechanical force-responsive systems face challenges in controlling and releasing encapsulated agents,[14] particularly in dental care applications where brushing or chewing occurs during oral hygiene practices.

Biopolymers such as alginate, chitosan, carrageenan, and shellac are widely used in healthcare products as carrier materials due to their non-toxicity, biodegradability, and biocompatibility.[15,16] Historically, shellac has been widely utilized as a preservative coating for fruit.[17] Shellac is typically dissolved in an alcohol-based solvent due to its solubility in polar solvents and applied to a substrate. Once the alcohol evaporates, the liquid shellac turns into a solid film. This principle has been adapted for the development of shellac-based encapsulation beads in the pharmaceutical and agricultural sectors.[18,19] Shellac's flexibility allows for a variety of encapsulation methods, including spray drying, precipitation, emulsion, and extrusion.[20] Its natural adhesive qualities, biodegradability, and non-toxicity meet the growing demand for sustainable and biocompatible materials in medical and dental applications.[21,22] In particular, shellac relies on phase separation in solvent systems to promote self-crosslinking within its non-polar domains,[23] whereas alginate and carrageenan require Ca^{2+} crosslinking to achieve film hardening,[24-26] and chitosan generally needs additional crosslinking agents.[27] Since F^-, as a small anion, cannot induce crosslinking, and Ca^{2+} binding is a critical concern in polysaccharide-based systems, shellac represents a more suitable choice for F^- encapsulation.

This study aims to present a straightforward extrusion method for fabricating shellac biopolymer beads for F^- encapsulation, demonstrating the calculated bead size and the release mechanism of F^- under mechanical stimulation. However, preliminary observations revealed that optimizing shellac's intrinsic physicochemical properties alone was insufficient to achieve the desired encapsulation efficiency. Surface defects were detected on the beads, likely caused by rapid solvent separation during solidification or irregularities in the polymer matrix, leading to F^- leakage. To address this limitation, a controlled reaction between F^- and Ca^{2+} was introduced, providing the first demonstration of an innovative *in situ* blocking approach that converts F^- into solid CaF_2 within the encapsulation matrix. This process effectively seals surface imperfections and demonstrates the synergistic role of CaF_2 in a novel encapsulation model with strong potential for toothpaste and other dental care applications, offering enhanced fluoride stability and efficacy.

2. Materials and methods

2.1. Materials

Wax-free shellac and calcium chloride ($CaCl_2$) were obtained from Sigma-Aldrich, United States of America (USA). Absolute ethanol (≥99.8%) and nitric acid were procured from Merck (Thailand), and sodium fluoride (NaF) was sourced from Ajax Chemical Ltd. (Australia). Glassware was pretreated by soaking in 0.5 M nitric acid, followed by cleaning with detergent and rinsing with deionized (DI) water. DI water served as the primary solvent throughout the study.

2.2. Sodium fluoride-shellac encapsulation preparation

An 80% w/v shellac solution was prepared by dissolving 8 g of shellac in 10 mL of absolute ethanol with gentle stirring for 5 days (shellac dissolution time). For shellac bead formation, a 5,000 ppm NaF solution was introduced into 10 mL of the shellac solution using a syringe pump (NE-300; New Era Pump Systems, USA) at a rate of 500 μL/min through an extrusion tube with a 0.4 mm diameter (27G flat needle, Nipro Medical, Japan). The NaF droplets within the shellac solution were incubated without stirring for 1 min (bead formation time), resulting in bead formation. The beads were subsequently transferred to DI water and incubated for 2 h (bead hardening time) before immersion in 10 mL of 5% $CaCl_2$. The shellac beads were then dried under ambient conditions. The process is illustrated schematically in Figure S1.

2.3. Material characterization

Before analysis, shellac beads were bisected along their diameter using a razor blade, rinsed with DI water, affixed to aluminum stubs with carbon tape, and vacuum-dried for 30 minutes. A charge-coupled device camera attached to an optical microscope (OM; AxioCam HRc, Carl Zeiss, Germany) was used to analyze the size distribution and wall thickness of shellac beads. Surface morphology was characterized using scanning electron microscopy (SEM; JSM-6510A, JEOL, Japan) in secondary electron imaging mode, with energy-dispersive X-ray spectroscopy (EDS) for elemental composition analysis. Functional groups were identified using Fourier-transform infrared spectroscopy (FTIR; Nicolet 6700 spectrometer, Thermo Scientific, USA) in attenuated total reflection (ATR) mode with a zinc selenide prism (IRK-FTS, Harrick, USA) over the 700–4,000 cm^{-1} spectral range. Crystallinity was assessed using differential scanning calorimetry (DSC; TGA/DSC 1, Mettler Toledo, Switzerland) at a heating rate of 10°C/min. Active fluoride content was measured indirectly using a waterproof fluoride meter (FL700, Extech, USA).

2.4. Statistical analysis

To evaluate encapsulation performance, statistical analyses were conducted using R version 4.4.2 (R Core Team, r-project.org). The Agricolae package was utilized to perform one-way

[1]Department of Mining and Materials Engineering, Faculty of Engineering, Prince of Songkla University, Hat Yai, Songkhla, Thailand; [2]Dental Clinic, Khok Pho Hospital, Khok Pho, Pattani, Thailand; [3]Sensor Research Unit, Department of Chemistry, Faculty of Science, Chulalongkorn University, Bangkok, Thailand; [4]Division of Physical Science, Faculty of Science, Prince of Songkla University, Hat Yai, Songkhla, Thailand

analysis of variance (ANOVA) to compare the effects during the observation period.[28-30]

3. Results and discussion

3.1. Shellac bead formation

Encapsulated shellac beads were continuously produced through syringe pump-driven extrusion, yielding a narrow size distribution and ensuring reproducibility. Further investigation into the primary shape-forming mechanism during this process is necessary. **Figure 1A** illustrates the morphology of the beads, which had an average particle diameter of 2.54 ± 0.22 mm (**Figure 1B**). The OM inset in **Figure 1A** shows the bead wall, revealing non-uniform thickness (163 ± 31 μm at the thinnest to 314 ± 82 μm at the thickest), caused by gravitational effects during bead formation. Moreover, the particle size distribution (**Figure 1B**) was assessed using the coefficient of variation, calculated as the percentage ratio of standard deviation to number-average diameter.[31] The extruded beads exhibited a coefficient of variation of 8.66%, which is less than 10%, indicating a narrow size distribution.[32]

To elucidate the influence of extrusion tube limitations, the dripping-in-laminar-flow model of NaF solution was adopted.[33] A syringe pump was utilized to control the flow rate, and drop formation was analyzed specifically employing Tate's law. Equation (1) offers a suitable approach for estimating particle diameter.[34,35]

$$V_{drop} = \frac{2\pi R\gamma}{\rho g} \quad (1)$$

According to Tate's law, drop volume (V_{drop}) is directly proportional to the extrusion tube radius (R) and influenced by solution surface tension (γ), density (ρ), and gravitational acceleration (g). This theoretical relationship has been experimentally validated using different nozzle sizes in related systems.[36] Assuming a spherical drop morphology, the estimated V_{drop} was utilized to predict particle diameter, employing the parameters shown in Table S1. For a NaF solution extruded through a 0.4 mm tube, the calculated drop diameter was 2.60 mm. This theoretical prediction showed 82% agreement with the experimentally measured internal spherical diameter (approximately 2.20 mm) from OM images (**Figure 1**). These findings, corroborated by diameter size simulations (Figure S2), underscore the critical influence of extrusion diameter on regulating particle size.

Moreover, the minimum force required to rupture the membrane (F) was estimated using the thin-walled spherical model (Equation (2)), which is based on tensile strength (σ), wall thickness (t), and bead radius (r).[37]

$$F = 2\pi\sigma tr \quad (2)$$

For pure thin-film shellac with a tensile strength of 1.86 MPa,[38] the breaking force calculated from the average bead diameter and minimum wall thickness was 2.38 N. This value falls within the typical range of tooth-brushing forces (1.5–3.5 N),[39] suggesting that shellac beads are highly susceptible to rupture during oral hygiene practices. According to Equation (2), reducing bead diameter proportionally decreases the required breaking force, increasing the likelihood of solution release and highlighting the challenges of miniaturizing shellac beads through nozzle extrusion. Future studies should experimentally validate this size dependence to confirm the predictions and extend the applicability of the findings.

To investigate the bead formation mechanism, molecular interactions between shellac and ethanol were examined using ATR-FTIR spectroscopy, as shown in **Figure 2**. An 80% w/v shellac solution was cast onto an ATR prism, allowing ethanol to evaporate under ambient conditions, leading to film formation. Time-dependent changes in the molecular structure of the shellac during ethanol evaporation were monitored using the ATR-FTIR technique (**Figure 2A**). Four characteristic peaks of ethanol were observed, as indicated by the black dashed line in **Figure 2A**, at 2,972, 1,260–1,050, and 880 cm^{-1}, corresponding to C–H stretching, C–O stretching, and O–H bending vibrations, respectively.[40,41] During the evaporation process, the ethanol-associated peak remained detectable until film formation was complete. Once the shellac film had fully formed, these peaks disappeared, while the characteristic vibrational bands of shellac remained unchanged and consistent with those of the original material. These observations indicate that ethanol was effectively removed during evaporation, facilitating shellac film formation.

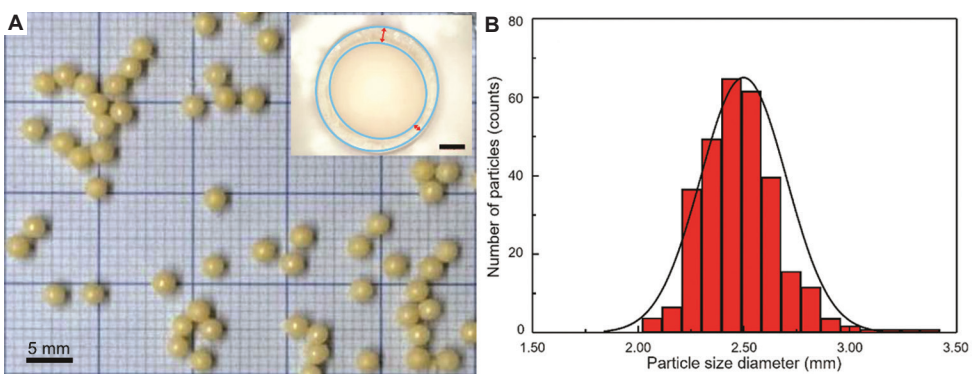

Figure 1. Morphology of the shellac beads. (A) Macroscopic image of sodium fluoride-encapsulated shellac beads on a grid (scale bar: 5 mm; magnification: ×2), with an inset microscopic image showing the bead wall and thickness variation (scale bar: 0.50 mm; magnification: ×10). (B) Size distribution of 300 fabricated shellac beads.

Figure 2B presents the ATR-FTIR spectra of shellac in its original form, as a film, and as beads after immersion in DI water for 7 days. The characteristic shellac peaks (gray dashed line in **Figure 2B**) were identified. The peaks at 2,928 and 2,852 cm^{-1} correspond to C–H stretching vibrations, while the peaks at 1,708 and 1,250 cm^{-1} correspond to stretching vibrations of the carbonyl group and the C–O bond of ester groups, respectively.[42] The results reveal no significant spectral changes, suggesting that ethanol dispersion from the shellac solution into the aqueous phase resulted in the formation of beads.

Molecular insights gained during the drying process underscore the role of solvent concentration gradients in shellac formulation. When a secondary solvent is introduced into the liquid shellac, ethanol diffuses into the secondary solvent due to concentration gradients. Consequently, a solid shellac bead forms, encapsulating the secondary solvent. The utilization of both static and dynamic chemical gradients facilitates molecular transport within swollen crosslinked polymers, a widely recognized mechanism for polymer hardening.[43] Based on the combined findings from OM and vibrational spectroscopy, the shellac encapsulation process can be described as driven by solvent separation, as shown in **Figure 3**.

3.2. Shellac encapsulation parameters

The extrusion method successfully formed microspherical shellac encapsulations, with the bead-forming mechanism detailed in the previous section. While the efficiency of NaF encapsulation within these shellac beads was subsequently monitored and recorded, further investigation into the parameters influencing shellac encapsulation is necessary. To optimize the conditions for shellac bead formation, key parameters, including shellac concentration, dissolution time, bead formation time, and hardening time, were systematically investigated. Encapsulation efficiency was quantified by determining the percentage of active F^- (AFs) retained within the beads using Equation (3):

$$\%AFs = \left(\frac{F^-_{initial} - F^-_{final}}{F^-_{initial}} \right) \times 100 \quad (3)$$

The F^- concentration in the stock solution ($F^-_{initial}$) and the concentration released from crushed shellac beads into DI water (F^-_{final}) were analyzed using the waterproof fluoride meter. The volume of the encapsulated bead, required for calculating F^-_{final}, was determined using spherical-diameter measurements of the inner structure, approximately 2.20 mm, as observed in the macroscopic image shown in **Figure 1**. The optimal conditions for shellac bead formation were identified based on a high percentage of AFs, reflecting superior shellac encapsulation performance, as shown in **Figure 4**. Measurements of F^-_{final} and %AFs were taken every 24 h for 7 days, with average and standard deviation values calculated using three beads per variable. DI water was used as the release medium to ensure accurate monitoring of loading solution loss from within the shellac beads.

To determine the optimal conditions for shellac bead formation, four key parameters were evaluated. **Figure 4A** presents the effect of shellac concentration. Shellac solutions above 80% w/v were difficult to prepare due to high viscosity

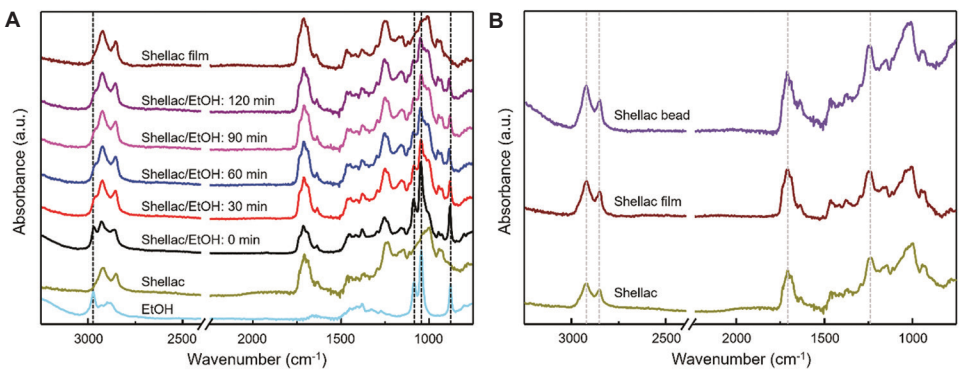

Figure 2. Molecular information during shellac drying. (A) Time-dependent attenuated total reflectance-Fourier-transform infrared spectroscopy (ATR-FTIR) spectra of shellac film cast from an 80% ethanolic shellac solution and dried under ambient conditions, compared to ethanol and original shellac. (B) ATR-FTIR spectra of original shellac, shellac film, and shellac beads after 7 days in deionized water.

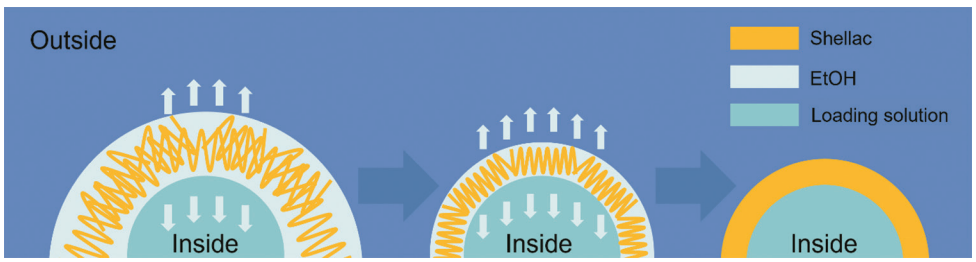

Figure 3. Schematic diagram of shellac bead hardening in deionized water.
Abbreviation: EtOH: Ethanol

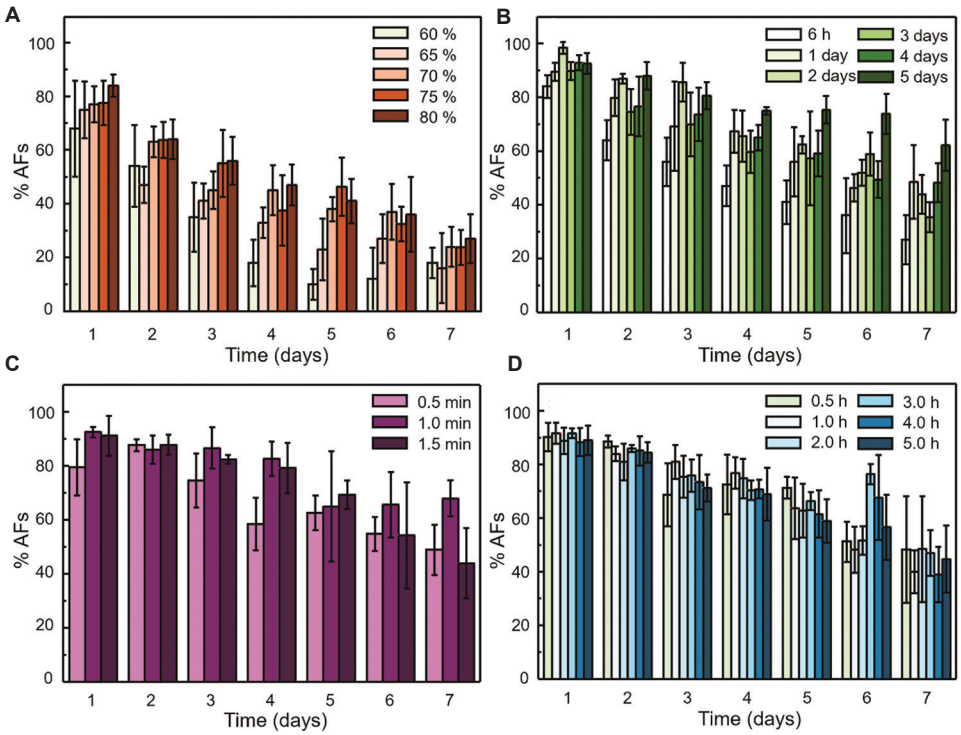

Figure 4. The percentage of active F^- in shellac beads encapsulated under different (A) shellac concentrations, (B) shellac dissolution times, (C) bead formation times, and (D) bead hardening times.

and slow dissolution. An 80% w/v stock solution was diluted to concentrations ranging from 75% to 60% w/v. Nevertheless, the 80% w/v shellac solution yielded the highest performance, retaining over 80% AFs. At 70% w/v, large surface pores (~5 μm; Figure S3) were observed, likely caused by lower viscosity facilitating rapid ethanol diffusion and leading to larger pore formation.[44]

Dissolution time significantly impacts the stretching and swelling of shellac polymer chains, influencing polymer integrity.[45] **Figure 4B** shows dissolution times ranging from 6 h to 5 days. A 5-day dissolution time resulted in over 85%AFs, with no significant improvement observed when extended to 7 days. Polymer chain expansion in solution influences crystallinity.[46,47] DSC was used to examine shellac beads prepared with dissolution times of 1 and 5 days (Figure S4). The DSC thermograms reveal a sharper endothermic peak for beads with a 5-day dissolution time compared to those with a 1-day dissolution time, indicating more uniform packing.[48] Therefore, a 5-day dissolution time was considered optimal for achieving efficient encapsulation.

Bead formation time, defined as the duration shellac beads remained in the ethanolic solution before transfer to DI water, was varied between 0.5 and 1.5 min (**Figure 4C**). A formation time of 1 min yielded over 85% AFs. At 0.5 min, the beads did not develop adequate wall thickness, preventing proper formation. At 1.5 min, the beads became soft and prone to cracking, leading to potential re-dissolution in the ethanolic shellac solution, and hindering successful transfer to DI water.

Following bead formation, shellac beads were immersed in DI water to stabilize their soft outer surface. Hardening time was critical for enhancing surface rigidity, promoting pore sealing, and maintaining structural integrity. Hardening times ranging from 0.5 to 5 h were evaluated (**Figure 4D**). A hardening time of 2 h resulted in optimal performance, with over 80%AFs, providing a balance between encapsulation efficiency and bead morphology.

Although the optimization process enhanced %AFs and encapsulation efficiency of the shellac beads, surface pores and F^- leakage were still observed. As illustrated in **Figure 4**, a decrease of approximately 20–30% AFs was noted from day 2 to day 7 compared to day 1. Beyond polymer hardening, pore formation on shellac bead surfaces, as shown in the schematic diagram (**Figure 3**), plays a critical role in encapsulation and release behavior. Pores generally arise during solvent evaporation or phase separation, where differential diffusion of polymer, solvent, and non-solvent phases drives void nucleation and growth.[49,50] Volatile loss may also generate internal stresses, leading to microcracks and increased surface porosity.[51] Drying kinetics further influence pore evolution: rapid evaporation tends to trap voids, whereas slower drying allows polymer chains to relax and densify.[52,53] To overcome this limitation, pore sealing was investigated to enhance NaF-shellac bead encapsulation. This modification and its effects are discussed in the subsequent section.

3.3. The role of calcium ions

Under the experimental conditions, shellac self-assembled from a liquid to a solid state on the bead surface due to the removal of ethanol from the shellac matrix. The resulting shellac beads exhibited regular morphology and composition (**Figures 1** and **2**). Nevertheless, the %AFs results

(**Figures 4A-D**) indicate that these thin-walled shellac beads are unsuitable for NaF encapsulation. SEM images of optimized shellac beads (**Figure 5A** and **B**) reveal small surface pores, <1 μm in diameter, both before and after immersion in DI water. While shellac-based nanoencapsulation has proven effective in other applications,[54,55] the presence of sub-micrometer pores highlights limitations in retaining loaded solutions, likely contributing to defects during the formation of microscale particles.[56]

To mitigate fluoride loss through surface pores, a stabilization strategy using Ca^{2+} was developed. Ca^{2+} was selected due to its biocompatibility, established use in oral care formulations, and its ability to react with F^- to form insoluble CaF_2,[57] thereby enhancing fluoride retention through *in situ* precipitation within the beads. $CaCl_2$ was selected as the Ca^{2+} source due to its widespread use in oral care products.[58] The reaction is presented in Equation (4), demonstrating the low stability of CaF_2 in water ($K_{sp} = 4.0 \times 10^{-11}$).[59,60]

$$2NaF_{(aq)} + CaCl_{2(aq)} \rightarrow 2NaCl_{(aq)} + CaF_{2(s)} \quad (4)$$

A prototype high-calcium toothpaste contains $CaCl_2$ at ~2.5% w/w, reported as the upper range for minimizing excessive Ca^{2+} reactivity.[61] Nevertheless, this concentration was insufficient for effective pore sealing in the shellac-wall beads, as only ~50% AFs was retained after 1 week, indicating limited sealing performance, which was confirmed by SEM imaging (Figure S5). To address this limitation, an increased concentration of 5% w/w $CaCl_2$ was investigated and demonstrated greater effectiveness in sealing pores. SEM analysis demonstrated that immersion of shellac beads containing F^- in 5% w/v $CaCl_2$ solution resulted in the formation of white circular deposits on the bead surface (**Figure 5C**). This process effectively sealed surface pores, in contrast to the porous structure observed in untreated beads (**Figure 5A** and **B**).

The reaction between NaF and $CaCl_2$ is rapid and spontaneous, resulting in the formation of insoluble CaF_2 (**Figure 6A**).[62] EDS mapping, shown in **Figure 6B-E**, was conducted to verify the chemical composition of the newly formed structures observed in **Figure 5C**. The EDS spectra confirmed the presence of calcium (Ca) and fluorine (F) atoms at 0.82 ± 0.36% and 1.98 ± 0.12%, respectively (**Figure 6F**), indicating that the white deposits consist of CaF_2. Additionally, carbon (C) and oxygen (O) atoms originating from the shellac material were detected.

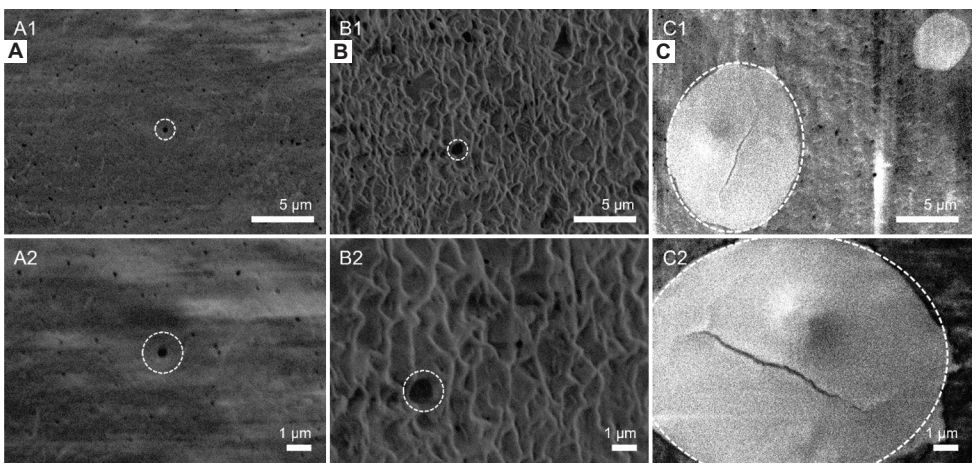

Figure 5. Scanning electron microscopic imaging of bead surface (A) before immersion, (B) after immersion in deionized water for 7 days, and (C) after immersion in 5% w/v $CaCl_2$ for 7 days. Scale bars: (A1, B1, C1) 5 μm, (A2, B2, C2) 1 μm; magnification: (A1, B1, C1) ×2000, (A2, B2, C2) ×5000.

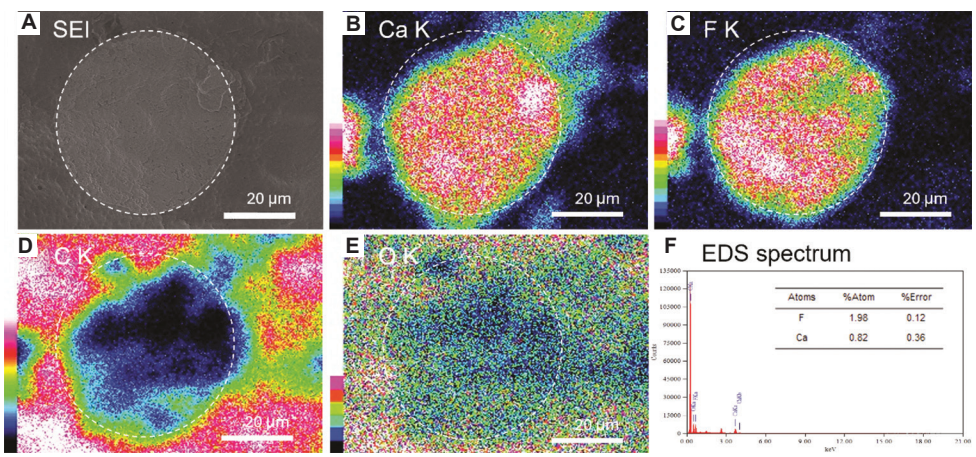

Figure 6. Elemental composition analysis on the bead surface. (A) Secondary electron image (SEI) of the bead surface; (B-E) Energy-dispersive X-ray spectroscopy (EDS) maps of Ca, F, C, and O. Ca K, F K, C K, and O K refer to Kα emission lines detected via EDS mapping; and (F) EDS spectrum of a shellac bead immersed in 5% w/v $CaCl_2$ for 7 days showing Ca and F atomic percentage.

Notably, the CaF_2 structures on the bead surface measured approximately 10–50 μm, substantially larger (10–50 times) than the original surface pores (less than 1 μm) observed in **Figure 5A** and **B**.

A plausible mechanism for CaF_2 formation is that F^- migrates through small pores and diffuses across the bead surface through capillary forces, reacting with Ca^{2+} to form a CaF_2 layer. This interaction, driven by the cooperative effect of CaF_2 and shellac, effectively seals the pores. SEM images and EDS maps (Figure S6) of the bead cross-section reveal that CaF_2 is present not only on the bead surface but also within tubular defects of the shellac wall. This finding confirms the robust pore-blocking capability of CaF_2 within the shellac encapsulation matrix. A schematic illustration based on SEM and EDS results is presented in **Figure 7**, offering insights into further optimization and demonstrating the potential of this approach for effective fluoride encapsulation.

3.4. The efficiency of calcium fluoride blocking

Calcium fluoride is essential for sealing surface pores to prevent the loss of encapsulated loading solutions within shellac beads. Under the optimal conditions established in Section 3.2, shellac beads were subjected to extreme conditions and immersed in 5% w/v $CaCl_2$, as shown in **Figure 8**. The %AFs were monitored daily for the first 14 days (14 measurements), weekly from days 15 to 35 (3 measurements), and then on days 60 and 90 (1 measurement each). The %AFs within the beads remained high—close to 80%—during the first 6 days (blue dots in **Figure 8**).

According to the results described in Section 3.2, shellac beads without CaF_2 co-blocking initially retained high %AFs (>80%) within 3 days, followed by a pronounced decline in %AFs thereafter. In contrast, only a slight decrease in %AFs was observed between days 7 to 90 for CaF_2-treated beads (black dots in **Figure 8)**. The average reduction in %AFs was 70%, with a relative standard deviation of 5%, which is within the acceptable range for quality control samples (≤ 15%).[63] This reduction may be attributed to the conversion of F^- to CaF_2 during the pore-sealing process. Furthermore, the %AFs remained a consistent range from days 7 to 90, running parallel to the horizontal axis (red line in **Figure 8**), suggesting no significant correlation between %AFs and immersion duration.[64] Levene's test confirmed homogeneity of variances across groups. A one-way ANOVA analysis conducted for the stability study revealed no significant differences at the 95% confidence level (p=0.80) among beads encapsulated from days 7 to 90, indicating stable and consistent fluoride retention throughout the storage period.[65]

These stability results confirm that, following 6 days of immersion, no continuous reaction occurred between F^- and Ca^{2+}. This observation is supported by the insignificant changes in %AFs within the Ca^{2+} reservoir, suggesting that this model is suitable for formulations containing Ca^{2+} compounds. The results demonstrate the high stability of CaF_2 integrated with shellac, ensuring sufficient encapsulation for extended shelf life. The retention of F^- within the shellac beads confirms the *in situ* pore-blocking function of CAF_2 as demonstrated in Equation (4). Blocking of surface pores and tubular shellac-wall

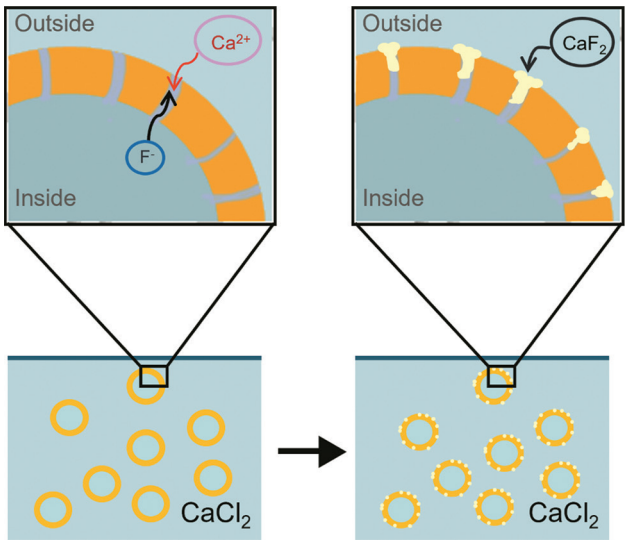

Figure 7. Proposed mechanism of the formation of calcium fluoride (CaF_2) on the bead surface.

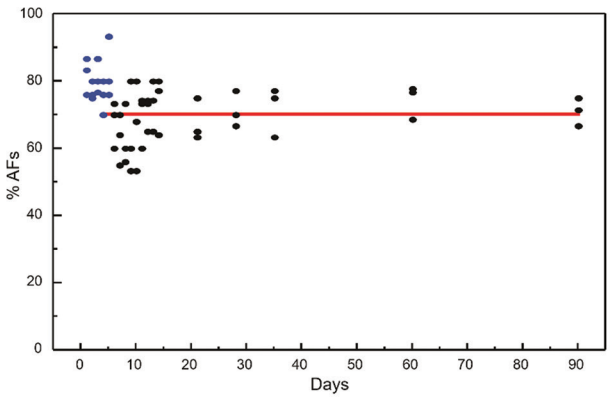

Figure 8. The percentage of active F^- (%AFs) encapsulated in shellac beads after 90 days in 5% $CaCl_2$. Blue dots represent days 1–6; black dots represent days 7–90, with the red line indicating the average %AFs.

structures by CaF_2 was clearly visible in SEM images and EDS maps. After the initial stabilization period, F^- levels stabilized and remained constant for up to 90 days, demonstrating the long-term efficacy of the CaF_2–shellac model for encapsulation in toothpaste applications.

4. Conclusions

This study presents the successful development of a novel shellac-based encapsulation model integrating CaF_2, engineered to enhance the stability of F^- for toothpaste applications. The employed method yielded shellac beads characterized by a narrow size distribution, suitable for fluoride loading. Analytical characterization confirmed the *in situ* generation of CaF_2 within the encapsulation matrix, which effectively sustained F^- levels at approximately 70% for up to 90 days, thereby substantially mitigating reactivity with exogenous calcium. This study focused solely on physicochemical characterization; dynamic oral factors such as artificial saliva, protein adsorption, and microbial metabolism were not assessed. Future *in vivo* or preclinical studies are needed to confirm translational relevance and potential applicability to other oral care products.

Acknowledgement

The authors would like to acknowledge Dr. Wisansaya Jaikeandee for her valuable assistance with visualization and illustration.

Financial support

This research was supported by the Thailand Science Research and Innovation Fund Chulalongkorn University, and NANOTEC (a member of NSTDA) under the Research Network of NANOTEC (RNN) program. A. Phengdaam would like to thank the Faculty of Science, Prince of Songkla University, for partially financial support.

Conflicts of interest statement

The authors declare that they have no known competing financial interests or personal relationships that could appear to have influenced the work reported in this paper.

Author contributions

Conceptualization: PP and AP; *Data curation:* PD; *Formal analysis:* PD; *Methodology*: PD, SE, PP, and AP; *Investigation*: PD; *Project administration*: PP *Supervision:* PP; *Visualization:* PD and AP; *Writing—original draft*: PD and CS; *Writing—review & editing:* PP and AP. All authors have read and agreed to the published version of the manuscript.

Ethics approval and consent to participate

Not applicable.

Consent for publication

Not applicable.

Availability of data

Data are available from the corresponding author on reasonable request.

References

1. Fejerskov O, Nyvad B, Kidd E. *Dental Caries: The Disease and Its Clinical Management.* United States: John Wiley and Sons; 2015. doi: 10.1038/s41415-025-8727-y
2. Buzalaf MA.R. *Fluoride and the Oral Environment.* Abingdon: Karger Medical and Scientific Publishers; 2011. doi: 10.1159/isbn.978-3-8055-9659-6
3. Tubert-Jeannin S, Auclair C, Amsallem E, *et al.* Fluoride supplements (tablets, drops, lozenges or chewing gums) for preventing dental caries in children. *Cochrane Database Syst Rev.* 2011;2011(12):CD007592. doi: 10.1002/14651858.cd011850.pub2
4. Hoxha A, Gillam DG, Agha A, *et al.* Novel fluoride rechargeable dental composites containing MgAl and CaAl layered double hydroxide (LDH). *Dent Mater.* 2020;36(8):973-986. doi: 10.1016/j.dental.2020.04.011
5. Dupare R, Kumar P, Dupare A, Jain R, Chitguppi R. Intraoral slow-release fluoride devices. *Int J Clin Prev Dent Res.* 2014;1:37-41.
6. Siriruk N, Rudee S, Varangkanar J, *et al.* Guideline on use of fluoride in dentistry. *J Dent Assoc Thai.* 2023;73(2):92-103. doi: 10.14456/jdat.2023.11
7. Bijella MFTB, Brighenti FL, Bijella MFB, Buzalaf MAR. Fluoride kinetics in saliva after the use of a fluoride-containing chewing gum. *Braz Oral Res.* 2005;19:256-260. doi: 10.1590/s1806-83242005000400004
8. Santos MG, Carpinteiro DA, Thomazini M, *et al.* Coencapsulation of xylitol and menthol by double emulsion followed by complex coacervation and microcapsule application in chewing gum. *Int Food Res.* 2014;66:454-462. doi: 10.1016/j.foodres.2014.10.010
9. Hattab FN. The state of fluorides in toothpastes. *J Dent.* 1989;17(2):47-54. doi: 10.1016/0300-5712(89)90129-2
10. Wason SK, Inventor JM. *Huber Corporation, Assignee. High Fluoride Compatibility Dentifrice Abrasives and Compositions.* U.S. Patents No. 4,340,583; 1982.
11. Nedovic V, Kalusevic A, Manojlovic V, Levic S, Bugarski B. An overview of encapsulation technologies for food applications. *Procedia Food Sci.* 2011;1:1806-1815. doi: 10.1016/j.profoo.2011.09.265
12. Rabanel JM, Banquy X, Zouaoui H, Mokhtar M, Hildgen P. Progress technology in microencapsulation methods for cell therapy. *Biotechnol Prog.* 2009;25(4):946-963. doi: 10.1002/btpr.226
13. Comunian TA, Favaro-Trindade CS. Microencapsulation using biopolymers as an alternative to produce food enhanced with phytosterols and omega-3 fatty acids: A review. *Food Hydrocoll.* 2016;61:442-457. doi: 10.1016/j.foodhyd.2016.06.003
14. Ma P, Lai X, Luo Z, *et al.* Recent advances in mechanical force-responsive drug delivery systems. *Nanoscale Adv.* 2022;4(17):3462-3478. doi: 10.1039/d2na00420h
15. Foglio Bonda A, Candiani A, Pertile M, Giovannelli L, Segale L. Shellac gum/carrageenan alginate-based core-shell systems containing peppermint essential oil formulated by mixture design approach. *Gels.* 2021;7(4):162. doi: 10.3390/gels7040162
16. Thombare N, Kumar S, Kumari U, *et al.* Shellac as a multifunctional biopolymer: A review on properties, applications and future potential. *Int J Biol Macromol.* 2022;215:203-223. doi: 10.1016/j.ijbiomac.2022.06.090
17. Miranda M, Sun X, Ference C, *et al.* Nano-and micro-carnauba wax emulsions versus shellac protective coatings on postharvest citrus quality. *J Am Soc Hortic Sci.* 2021;146(1):40-49. doi: 10.21273/jashs04972-20
18. Yuan Y, He N, Dong L, *et al.* Multiscale shellac-based delivery systems: From macro- to nanoscale. *ACS Nano.* 2021;15(12):18794-18821. doi: 10.1021/acsnano.1c07121
19. Zabot GL, Schaefer Rodrigues F, Polano Ody L, *et al.* Encapsulation of bioactive compounds for food and agricultural applications. *Polymers (Basel).* 2022;14(19):4194. doi: 10.3390/polym14194194
20. Chen Y, Zhu Z, Shi K, *et al.* Shellac-based materials: Structures, properties, and applications. *Int J Biol Macromol.* 2024;279:135102. doi: 10.1016/j.ijbiomac.2024.135102
21. Baxmann M, Baráth Z, Kárpáti K. Application and future utilization of shellac in orthodontics: A systematic review. *J Clin Med.* 2024;13(10):2917. doi: 10.3390/jcm13102917
22. Hoang-Dao BT, Hoang-Tu H, Tran-Thi NN, *et al.* Clinical efficiency of a natural resin fluoride varnish (Shellac F) in reducing dentin hypersensitivity. *J Oral Rehabil.* 2009;36(2):124-131. doi: 10.1111/j.1365-2842.2008.01907.x
23. Sharma S, Samrat, Goyal P, *et al.* Shellac: Bridging the gap between chemistry and sustainability-a comprehensive review of its multifunctional coating applications for food, drug, and paper packaging. *J Macromol Sci Part A.* 2024;61(10):691-723. doi: 10.1080/10601325.2024.2400510
24. Martău GA, Mihai M, Vodnar DC. The use of chitosan, alginate, and pectin in the biomedical and food sector-biocompatibility, bioadhesiveness, and biodegradability. *Polymers (Basel).* 2019;11(11):1837. doi: 10.3390/polym11111837
25. Li L, Fang Y, Vreeker R, Appelqvist I, Mendes E. Reexamining the egg-box model in calcium- alginate gels with X-ray diffraction. *Biomacromolecules.* 2007;8(2):464-468. doi: 10.1021/bm060550a
26. Tako M, Teruya T, Tamaki Y, Uechi K, Konishi T. Molecular origin for strong agarose gels: Multi-stranded hydrogen bonding. *J Polym Biopolym Phys Chem.* 2021;9:13-19. doi: 10.12691/jpbpc-9-1-2
27. Detsi A, Kavetsou E, Kostopoulou I, *et al.* Nanosystems for the encapsulation of natural products: The case of chitosan biopolymer as a matrix. *Pharmaceutics.* 2020;12(7):669. doi: 10.3390/pharmaceutics12070669
28. Lüdecke D. Ggeffects: Tidy data frames of marginal effects from regression models. *J Open Source Softw.* 2018;3(26):772. doi: 10.21105/joss.00772
29. Mendiburu FD, Simon R. Agricolae-ten years of an open source statistical tool for experiments in breeding, agriculture and biology. *PeerJ.* 2015;3:e1404v1.

doi: 10.7287/peerj.preprints.1404v1
30. Noppradit B, Uthaipan N, Klinnawee L, Kongtragoul P, Phengdaam A. Antifungal copper nanocomposite-rubber compound for tree wound dressings. *Ind Crops Prod.* 2024;222:119798. doi: 10.1016/j.indcrop.2024.119798
31. Sugiura S, Nakajima M, Seki M. Preparation of monodispersed polymeric microspheres over 50 μm employing microchannel emulsification. *Ind Eng Chem Res.* 2002;41(16):4043-4047. doi: 10.1021/ie0201415
32. Tang L, Fan TM, Borst LB, Cheng J. Synthesis and biological response of size-specific, monodisperse drug-silica nanoconjugates. *ACS Nano.* 2012;6(5):3954-3966. doi: 10.1021/nn300149c
33. Ning S, Long Y, Zhao Y, *et al.* Research on micro-liquid dispensing driven by a syringe pump with the consideration of air volume. *Microsyst Technol.* 2021;27:3653-3666. doi: 10.1007/s00542-020-05133-9
34. Lee BB, Ravindra P, Chan ES. A critical review: Surface and interfacial tension measurement by the drop weight method. *Chem Eng Commun.* 2008;195(8):889-924. doi: 10.1080/00986440801905056
35. Hou B, Wu C, Liu H, *et al.* Shape approximation of sessile droplet by the equivalence between vertical capillary force and hydrostatic pressure. *Colloids Surf A Physicochem Eng Asp.* 2023;656:130203. doi: 10.1016/j.colsurfa.2022.130203
36. Hernandez-Aguilar JR, Cunningham R, Finch JA. A test of the Tate equation to predict bubble size at an orifice in the presence of frother. *Int J Miner Process.* 2006;79(2):89-97. doi: 10.1016/j.minpro.2005.12.003
37. Ross CT. *Pressure Vessels: External Pressure Technology.* Netherlands: Elsevier; 2011. doi: 10.1533/9780857092496
38. Ghoshal S, Khan MA, Gul-E-Noor F, Khan RA. Gamma radiation induced biodegradable shellac films treated by acrylic monomer and ethylene glycol. *J Macromol Sci Part A.* 2009;46(10):975-982. doi: 10.1080/10601320903158594
39. Van der Weijden G, Timmerman M, Versteeg P, Piscaer M, Van der Velden U. High and low brushing force in relation to efficacy and gingival abrasion. *J Clin Periodontol.* 2004;31(8):620-624. doi: 10.1111/j.1600-051x.2004.00529.x
40. Mudalip SKA, Bakar MRA, Adam F, Jamal P. Structures and hydrogen bonding recognition of mefenamic acid form I crystals in mefenamic acid/ethanol solution. *Int J Chem Eng Appl.* 2013;4(3):124-128. doi: 10.7763/ijcea.2013.v4.277
41. Golub P, Doroshenko I, Pogorelov V, *et al.* Temperature evolution of cluster structures in ethanol. *Dataset Papers Sci.* 2013;2013:473294. doi: 10.1155/2013/473294
42. Yan G, Cao Z, Devine D, Penning M, Gately NM. Physical properties of shellac material used for hot melt extrusion with potential application in the pharmaceutical industry. *Polymers (Basel).* 2021;13(21):3723. doi: 10.3390/polym13213723
43. Ali MA, Volmert B, Evans CM, Braun PV. Static and dynamic gradient based directional transportation of neutral molecules in swollen polymer films. *Angew Chem Int Ed Engl.* 2022;61(41):e202206061. doi: 10.1002/anie.202206061
44. Strawhecker KE, Kumar SK, Douglas JF, Karim A. The critical role of solvent evaporation on the roughness of spin-cast polymer films. *Macromol.* 2001;34(14):4669-4672. doi: 10.1021/ma001440d
45. Miller-Chou BA, Koenig JL. A review of polymer dissolution. *Prog Polym Sci.* 2003;28(8):1223-1270. doi: 10.1016/S0079-6700(03)00045-5
46. Narasimhan B. Mathematical models describing polymer dissolution: Consequences for drug delivery. *Adv Drug Deliv Rev.* 2001;48(2-3):195-210. doi: 10.1016/s0169-409x(01)00117-x
47. Ito Y, Shiina S, Tokue I. Influence of expansion of polymer molecules in solution on non-newtonian flow behavior. *Makromol Chem.* 1982;183(2):505-510. doi: 10.1002/macp.1982.021830219
48. Yoo E, Im S. Melting behavior of poly(butylene succinate) during heating scan by DSC. *J Polym Sci Part B Polym Phys.* 1999;37(13):1357-1366. doi: 10.1002/(sici)1099-0488(19990701)37:13<1357::aid-polb2>3.0.CO;2-Q
49. Li H, Kruteva M, Mystek K, *et al.* Macro-and microstructural evolution during drying of regenerated cellulose beads. *ACS Nano.* 2020;14(6):6774-6784. doi: 10.1021/acsnano.0c00171
50. Wu D, Xu F, Sun B, *et al.* Design and preparation of porous polymers. *Chem Rev.* 2012;112(7):3959-4015. doi: 10.1021/cr200440z
51. Gokmen MT, Du Prez FE. Porous polymer particles-a comprehensive guide to synthesis, characterization, functionalization and applications. *Prog Polym Sci.* 2012;37(3):365-405. doi: 10.1016/j.progpolymsci.2011.07.006
52. Ballai G, Kotnik T, Finšgar M, *et al.* Highly porous polymer beads coated with nanometer-thick metal oxide films for photocatalytic oxidation of Bisphenol A. *ACS Appl Nano Mater.* 2023;6(21):20089-20098. doi: 10.1021/acsanm.3c03891
53. Fashandi H, Karimi M. Pore formation in polystyrene fiber by superimposing temperature and relative humidity of electrospinning atmosphere. *Polymer.* 2012;53(25):5832-5849. doi: 10.1016/j.polymer.2012.10.003
54. Yuan Y, Zhang S, Ma M, Xu Y, Wang D. Delivery of curcumin by shellac encapsulation: Stability, bioaccessibility, freeze-dried redispersibility, and solubilization. *Food Chem X.* 2022;15:100431. doi: 10.1016/j.fochx.2022.100431
55. Muhammad DRA, Doost AS, Gupta V, *et al.* Stability and functionality of xanthan gum-shellac nanoparticles for the encapsulation of cinnamon bark extract. *Food Hydrocoll.* 2020;100:105377. doi: 10.1016/j.foodhyd.2019.105377
56. Jangizehi A, Schmid F, Besenius P, Kremer K, Seiffert S. Defects and defect engineering in soft matter. *Soft Matter.* 2020;16(48):10809-10859. doi: 10.1039/d0sm01371d
57. Koeser J, Carvalho TS, Pieles U, Lussi A. Preparation and optimization of calcium fluoride particles for dental applications. *J Mater Sci Mater Med.* 2014;25(7):1671-1677. doi: 10.1007/s10856-014-5200-x
58. Wentink GA, Van Den Ingh TS. Oral administration of calcium chloride-containing products: Testing for deleterious side-effects. *Vet Q.* 1992;14(2):76-79. doi: 10.1080/01652176.1992.9694334
59. Kimura H, Kai J. Phase change stability of $CaCl_2$ $6H_2O$. *Sol Energy.* 1984;33(6):557-563. doi: 10.1016/0038-092X(84)90011-2
60. Fedorov P, Luginina AA, Alexandrov AA, Chernova EV. Transformation of calcite $CaCO_3$ to fluorite CaF_2 by action of KF solution. *J Fluor Chem.* 2021;251:109898. doi: 10.1016/j.jfluchem.2021.109898
61. Wu L, Li F, Morrow BR, *et al.* A novel antimicrobial and remineralizing toothpaste containing $CaCl_2$/chitosan microspheres. *Am J Dent.* 2018;31(3):149.
62. Markovic M, Takagi S, Chow LC, Frukhtbeyn S. Calcium fluoride precipitation and deposition from 12 mmol/L fluoride solutions with different calcium addition rates. *J Res Natl Inst Stand Technol.* 2009;114(5):293-301. doi: 10.6028/jres.114.021
63. Onyeabor F, Paik A, Kovvasu S, *et al.* Optimization of preparation and preclinical pharmacokinetics of celastrol-encapsulated silk fibroin nanoparticles in the rat. *Molecules.* 2019;24(18):3271. doi: 10.3390/molecules24183271
64. Mukaka MM. A guide to appropriate use of correlation coefficient in medical research. *Malawi Med J.* 2012;24(3):69-71.
65. Djira GD, Hothorn LA, Tsong Y. Equivalence tests for shelf life and average drug content in stability studies. *J Biopharm Stat.* 2008;18(5):985-995. doi: 10.1080/10543400802287230

Received: July 14, 2025
Revised: October 9, 2025
Accepted: October 17, 2025
Available online: November 19, 2025